

MOLECULAR-DYNAMICS STUDY OF THE LOCAL SYMMETRY CHANGES IN METALLIC LIQUIDS

M. KRETH^{a, *}, P. ENTEL^a, K. KADAU^b and R. MEYER^a

^a*Institute of Physics, University of Duisburg,
47048 Duisburg, Germany;*

^b*Los Alamos National Laboratory, T11, MS B262,
Los Alamos, NM 87545, U.S.A.*

(Received ...)

Abstract

It has been conjectured that the local structure of simple mono-atomic liquids is mainly of five-fold symmetry. Experimental evidence for such icosahedral building blocks has recently been found in liquid droplets of lead adjacent to a silicon wall and in deeply undercooled melts of pure metallic elements like bcc iron, fcc nickel and bcc zirconium. We have used molecular dynamics in order to investigate supercooling effects in the melt of another pure element (aluminum) on the basis of a common neighbor analysis. In the simulation we have employed an embedded atom method potential optimized with the help of *ab initio* calculations for aluminum. The simulations confirm the recent experimental results that, independent of the system, the icosahedral short-range order *strongly increases* with the degree of undercooling.

Keywords: Local symmetries in metallic melts, Undercooled aluminum, Molecular dynamics simulations,

*Corresponding author. E-mail: magnus@thp.uni-duisburg.de

1. INTRODUCTORY REMARKS ON METALLIC MELTS

The existence of undercooled melts has led to numerous experimental and theoretical activities since the pioneering work of Turnbull (1950). In particular the observation that the undercooled melts of pure metallic elements develop local structures such as icosahedrons having fivefold symmetry (Frank, 1952; Reichert *et al.*, 2000; Schenk *et al.*, 2002), which is incompatible with the two, three- four- or sixfold symmetries of the solid phases, has led to speculations about the structure of liquids and the nature of the solid-liquid transition and how to conceptually characterize this phase transition in terms of conserved (or non-conserved) order parameters. The local atomic structures in the melts become extremely complex in the case of alloy systems. Here the solid-liquid interface energy plays an important role in the solidification governing the microstructure fineness, the precursors of which probably develop already in the undercooled melts. Supercooled and amorphous-like alloy melts develop, in addition, a tendency to glassy behavior and glass-like phase transitions with a slowing down of the undercooled liquid's dynamics (until structural arrest is reached) (Rößler and Teichler, 2000; Faupel *et al.*, 2003). For such systems chemical short-range order at the level of tetrahedral clusters is often the prominent symmetry observed in the simulations and in experiments (Rößler and Teichler, 2000; Lamparter and Steeb, 1998).

In addition one should mention that the surface structure of both liquid metal and liquid metal alloy surfaces bears intriguing features being intensively discussed at present, for example, see Tostmann *et al.* (2000) and DiMasi *et al.* (2000). This is because liquid metals can be considered as a two-component fluid of nearly free electrons coupled by Coulomb interactions to the ions requiring a quantum mechanical treatment of the electrons (in contrast, for example, to dielectric liquids, which can be considered as a one-component fluid). The consequences are of macroscopic nature like a much larger surface tension of the liquid metals compared to dielectric liquids. Large surface tension means suppression of thermal fluctuations of the surface, i.e., liquid metals have flat surfaces created by the conduction electrons leading to layering of atoms near the surface and an associated specific electron density profile perpendicular to the surface. Layering has so far been observed only for the three liquid metals Ga, In and Hg, see discussion in (Tostmann *et al.*, 2000; DiMasi *et al.*, 2000) and (DiMasi *et al.*, 2001).

Summarizing one may say that the solidification and surface behavior of monoatomic systems is not completely understood; the solidification of alloy systems brings in new elements like constitutional undercooling, development of glassy behavior and formation of texture morphology and is even less understood.

When considering the reverse process (melting) one observes a distinct change of the coordination number z . For typical liquid metals z lies, as a general rule, between 9 and 11 (and is thus smaller than $z = 12$ for the close-packed fcc structure), which is due to the introduction of defects in the molten state. For those cases where the solid is not close packed (such as bcc crystals with $z = 8$ or the diamond structure with $z = 4$), the coordination number tends to increase upon melting. Although this may serve as a thumb rule, this classification is inadequate for a detailed analysis of the symmetry changes in metallic liquids and in the undercooled metallic melts. A more refined data analysis is required as discussed below.

The mobile, accidentally oriented fragments with fivefold symmetry cannot be observed in conventional scattering experiments for structure analysis. Only recently by using the scattering of totally internally reflected (evanescent) X-rays (being sensitive only to the liquid structure at the interface), Reichert *et al.* succeeded to prove the existence of small liquid droplets of lead with fivefold symmetry at a silicon interface (Reichert *et al.*, 2000). In another recent experiment combining electromagnetic levitation with neutron scattering icosahedral short-range order was observed in deeply undercooled melts of pure Fe, Ni and Zr (Schenk *et al.*, 2002) and of Co (Holland-Moritz *et al.*, 2002). In addition to these symmetry studies, magnetic properties of (in a gas flux) undercooled Co and Co-Au alloy melts have been recently investigated (Reutzel and Herlach, 2003). With respect to the simulation of undercooled melts the method of molecular dynamics (MD) is particularly suited. It has the advantage that symmetry changes in the melts can easily be studied and is, therefore, in addition to the experiment, a very helpful tool in such investigations.

Liquids were among the first systems to be studied widely by computer simulations, for references see (Allen and Tildesley, 1987). For example, the local structures in (supercooled) liquids have been investigated by Steinhardt *et al.* (1981) and Jónsson and Andersen (1988) by using simple pairwise additive Lennard-Jones potentials for the interaction of the atoms, which give less reliable results than the many-particle embedded atom method (EAM) potential used in this work.

The characterization of a liquid with respect to undercooling requires knowledge of the melting temperature T_m . A direct determination of T_m by heating the system up to the solid-liquid transition is hindered by the use of periodic boundary conditions, since the absence of surfaces usually allows an overheating of the solid phase far beyond the melting temperature. A widespread method to determine T_m relies on the evaluation of the free energies for the solid and liquid phases. A useful relation for the calculation of the free energy is (Morris *et al.*, 1994)

$$F = F_0 + \int_0^1 d\lambda \langle V - V_\lambda \rangle_\lambda, \quad (1)$$

where F is the free energy of the system with potential energy V and F_0 is the corresponding energy of an exactly solvable model system with potential energy V_0 ; the averaging in Eq. (1) is done with respect to the potential $V_\lambda = \lambda(V - V_0)$. With the help of a series of simulations for different V_λ a numerical evaluation of F can be achieved. The free energy for different temperatures can then be calculated using

$$\frac{F}{T} - \frac{F_0}{T_0} = \int_{T_0}^T d\tau \frac{E(\tau)}{\tau^2}. \quad (2)$$

While the calculation of F for a solid is not so problematic when using Eq. (1) and (2), the choice of an adequate reference system for the liquid phase is more difficult. When choosing the ideal gas as reference system, we can reach the desired state (on the integration path) by an isothermal expansion of the system volume. However, the path of integration in Eq. (1) must remain reversible, i.e., a phase transition is excluded. In order to circumvent this problem one can switch off the attractive part of the interaction and, in a second step, enlarge the volume until the system can be treated as a weakly interacting system. But this procedure requires many simulations. In addition, a precise determination of T_m from the crossing of the free energies of the solid and liquid phases requires a high accuracy of free energies: Errors of the order of 0.01 eV/atom give rise to errors in T_m of the order of 100 K (Foiles and Adams, 1989).

An alternative method, which has been used in this work, relies on a direct determination of the phase stability from a two-phase simulation (Morris *et al.*, 1994; Morris and Song, 2002). In such simulations the initial system contains both phases, i.e., solid and liquid part. In the subsequent simulation at fixed temperature the thermodynamic stable phase will grow on the

expense of the other phase. The melting point is then determined by the temperature for which the transition occurs from the temperature range of the stable solid to the temperature range of the stable liquid.

In this paper we concentrate on details of the temperature dependence of the local symmetries (atomic short-range order) in stable undercooled monoatomic metallic melts like Al on the basis of molecular-dynamics simulations using an optimized EAM potential for Al (Grabowski *et al.*, 2002). Our aim is to check, on the basis of the simulations, whether the increase of icosahedral short-range order with decreasing temperature, as observed in the experiment for bulk Fe, Co, Ni and Zr liquids (Schenk *et al.*, 2002), holds also for Al. To our knowledge most of the experiments and simulations have been devoted to the investigation of the short-range order in Al-based alloys forming quasicrystalline phases (Maret *et al.*, 1993; Simonet *et al.*, 1998, 2002) (here, additionally, magnetism and atomic short-range order are of interest since, for example, magnetic moments are present in the liquid state of Al-Pd-Mn alloys but not in the solid phase (Simonet *et al.*, 1998)).

2. MOLECULAR DYNAMICS

EAM potentials of the form proposed by Daw and Baskes (1984) have been successfully applied to describe lattice dynamics, lattice defects and dynamics of the liquid state in metals. In the EAM case, the potential energy of a single atom is considered as the energy required to embed the atom into the local electron density provided by the other atoms plus a core–core repulsion potential which takes the form of a pair potential. The potential energy is written as

$$E = \sum_i F(\rho_i) + \sum_{i<j} \Phi(r_{ij}), \quad (3)$$

where the summation is over all atoms and r_{ij} is the distance between the atoms i and j . The function $F(\rho_i)$ represents the embedding energy of atom i depending on the background charge density

$$\rho_i = \sum_{j \neq i} \rho_j^{at}(r_{ij}), \quad (4)$$

which is the sum over all atomic contributions $\rho_j^{at}(r_{ij})$ from the neighboring atoms. The second term in Eq. (3) represents a screened Coulomb potential,

$$\Phi(r) = 2 \frac{Z(r)Z(r)}{r}, \quad (5)$$

with the effective charge $Z(r)$. The factor 2 stems from the atomic units used in this paper.

In general the embedding function $F(\rho)$ is not known, therefore, an *ansatz* for $F(\rho)$ is chosen which is subsequently adjusted to experimental data. For the representation of $F(\rho)$ and $Z(r)$ cubic spline functions are usually used, the parameters of which are fixed by the experimental data for the lattice constant, binding energy, vacancy formation energy, elastic constants as well as selected zone boundary phonon frequencies. In addition, in the choice of potential parameters the equation of state, $E(V)$, obtained from *ab initio* calculations has been taken into account. Details of the fit procedure for the case of Al can be found in (Grabowski *et al.*, 2002). This additional fit to *ab initio* data leads to a potential which is softer at lower inter-particle distances than the corresponding interaction potential which is solely based on the experimental data describing the thermal equilibrium state of the metal. In particular this interaction allows the investigation of diffusion processes via vacancies in solid aluminum, yielding a temperature dependence for diffusion coefficient which is in reasonable agreement with experiment (Grabowski *et al.*, 2002). Therefore, this EAM potential is best suited for investigating the local symmetry changes in the undercooled liquid metal regime.

In the simulations we use the *velocity Verlet* algorithm with a time step of 1.5 fs for the integration of the equations of motion of the atoms; the Nosé-Hoover thermostat is employed for the control of the temperature and the Andersen method for the control of the pressure. For the methodical details we refer to the literature (Allen and Tildesley, 1987; Rapaport, 1995).

3. TWO-PHASE SIMULATIONS OF NANO-CLUSTERS

In this work so called two-phase simulations for solid Al particles of different sizes surrounded by liquid Al in a box with periodic boundary conditions were used to determine the melting temperature T_m of the particles. Then an extrapolation of the particle size to infinity allows to determine the melting

temperature of bulk Al, of which the experimental value is 933.52 K at 101325 Pa (Binder, 1999). Additionally we have calculated the calorific curves $E(T)$ for particles with different sizes in vacuo, where the jump in the $E(T)$ curve is a different way to identify T_m .

In the two-phase simulations we used a two-step preparation of the system, which consisted of an equilibration of 10976 atoms in $14 \times 14 \times 14$ fcc cells at 750 K and a subsequent increase of the temperature to 1200 K, during which the positions and velocities of all atoms in a central (with respect to the simulation box) sphere of diameter 46.6 Å were kept fixed. Then simulations were carried out for a span of time required to melt all mobile Al atoms around the frozen core atoms. This two-phase system was then used in the following MD simulations as start configuration.

At the beginning of each subsequent investigation we reduced the temperature gradient at the solid-liquid phase boundary by short simulations (100 integrations) using a ten times smaller time step of 0.15 fs. Because of the shortness of these runs no structural relaxation at the interface occurred. In the following MD simulations the number of steps was chosen such that at the end of each MD run the total system was either completely condensed or completely liquid which required individual simulations times up to 45 ps. The simulations were started at 880 K, for which the final state is the condensed one, and at 950 K, for which the final state is liquid. In the following further temperatures were chosen from this interval until the melting temperature (of the particle with 46.6 Å diameter) was restricted to a temperature interval of the order of 1 K. The resulting total energy as a function of the temperature is shown in Fig. 2. The jump in the curve between 908 and 909 K separates the temperature intervals in which the system condenses ($T \leq 908$ K) and in which it melts ($T \geq 909$ K). Accordingly the melting temperature of the system (initial solid core of diameter 46.6 Å surrounded by liquid Al) amounts to $T_m \approx 908.5 \pm 0.5$ K.

We have then repeated the simulation of coexisting phases for spherical solid particles with different diameters, 33.9 Å, 38.1 Å and 42.3 Å, in the liquid environment. For these systems we obtained for the melting temperatures 860.5 ± 0.5 K, 879.5 ± 0.5 K and 889.5 ± 0.5 K, respectively, which are plotted together with the value of $T_m \approx 908.5 \pm 0.5$ K for the 46.6 Å particle in Fig. 3. By assuming a linear decrease of the melting temperature with the inverse of the particle diameter (a linear relationship between the melting point lowering and the inverse of the particle diameter, $1 - T_m/T_B \propto 1/d$, where T_B is the bulk melting temperature, was postulated by Pawlow (1909a,b)

and experimentally confirmed by Coombes (1972), Buffat and Borel (1976) and Ben David *et al.* (1995)) and by extrapolating to very large particles we obtain a bulk melting temperature of $T_B \approx 1028$ K (not correcting for finite-size effects), which shows that in this simulation we overestimate T_B^{exp} by ca. 100 K. Nevertheless this value is still closer to the experimental value of 933 K than the underestimate of the melting temperatures obtained in previous calculations using different EAM potentials: $T_B = 800 \pm 10$ K was obtained in (Mei and Davenport, 1992) and $T_B = 724$ K (also a two-phase simulation) in (Morris *et al.*, 1994) (at $P = 0$); note that the significantly lower values of both calculations, compared to $T_B^{\text{exp}} \approx 933$ K, were attributed to the observation that the inaccurate melting temperature is assumed to be a common shortcoming of the EAM potentials (Foiles and Adams, 1989). We attribute the better agreement of our melting point with the experimental value to the fact that our potential, due to the additional fit to the *ab initio* data, displays much better the softer elastic behavior of the interacting Al atoms for shorter distances between them than the equilibrium distance.

On the other hand this work shows that even by fitting the potential to *ab initio* results it seems to be hard to obtain correct melting temperatures for metallic melts. One reason may be that the EAM potentials, which retain electronic information in a semi-empirical way, cannot adequately describe the degree of compressibility and deformability of the shells of the valence electrons and that a full quantum mechanical treatment of the electrons of metals is required in order to obtain realistic melting temperatures. The discussion of the importance of a quantum mechanical treatment of the electrons when discussing the surfaces of liquid metals (DiMasi *et al.*, 2000) underlines this assumption.

The calorific curves not obtained from the two-phase simulations but from the simulations of free initially spherical-like Al particles (using the same optimized EAM potential) with different sizes in vacuo show a rather sharp increase with increasing temperature at T_m comparable to the behavior of $E(T)$ in Fig. 2. In this case the extrapolation to infinite particle size gives a value of $T_B \approx 1030$ K for the bulk melting temperature, see Fig. 4, which is not too different from the result of the two-phase simulations. When heating the free nano-clusters we observe a variety of phase changes before the melting temperature is reached (shape fluctuations). Such fluctuations as well as related (stimulated and not stimulated) nano-cluster transformations (Rieth, 2003) will not be discussed here. Instead we will describe below the changes of the atomic short-range order in the undercooled liquid phase of

Al with decreasing temperature.

4. CHANGE OF THE LOCAL SYMMETRIES IN SUPERCOOLED LIQUIDS

For investigating the local structures in liquid Al we used the same simulation cell as before, i.e., a system consisting of 10976 atoms prepared in the solid phase (14^3 fcc cells with periodic boundary conditions). This system was heated up to 1500 K (melting set in at about 1300 K) in order to achieve a sufficient equilibration of the liquid state. Subsequently we cooled down the system to 1300 K, then to 1100 K and then from 1100 K to 600 K in steps of 100 K. At each temperature we carried out 25000 simulation steps with a time step of 1.46 fs (corresponding to a total time of 36.5 ps of the MD run). The system remains liquid down to 600 K.

In order to get information about the changes of the atomic short-range order with temperature we performed a *Common-Neighbor-Analysis* (CNA) (Honeycutt and Andersen, 1987; Jónsson and Andersen, 1988; Faken and Jónsson, 1994) for each temperature. In this analysis we used the over the last 1.5 ps averaged atomic positions, which guarantees that the CNA is not influenced by thermal fluctuations of the atomic positions. The CNA is a method allowing to characterize the coordination of neighbored atoms of a given pair of atoms. A pair of atoms at \mathbf{r}_i and \mathbf{r}_j is considered a “bound pair” (in the sense of the CNA) provided the distance $r_{ij} = |\mathbf{r}_i - \mathbf{r}_j|$ does not exceed a threshold value, i.e., $r_{ij} < r_c$, where r_c is usually the position of the first minimum of the radial distribution function (RDF). Three indices, klm , are then assigned to each bound pair of atoms (the CNA signature of the pair). Here the first index, k , is the number of neighbors common to both atoms. The second index, l , is the number of bonds between these common neighbors. In order to distinguish local structures having the same indices k and l like, for example, fcc and hcp structures, a third index m is used, which is the number of bonds in the longest continuous chain formed by the l bonds between the common neighbors. Then a CNA analysis for an fcc structure results in a 421 signature, whereas the hcp structure has equally many 421 and 422 signatures. After characterizing each pair of atoms by klm the distribution of distances can be calculated which allows to introduce

a radial distribution function, $g_{klm}(r)$, for each type of pairs. They can be considered as the CN components of the RDF and are normalized in such a way that the RDF can be written as (Faken and Jónsson, 1994)

$$g(r) = \sum_{klm} g_{klm}(r). \quad (6)$$

In a liquid, besides the typical signatures of close-packed structures, we find many other signatures, among which are 100, 200 and 311 pairs; they reflect the obvious fact that the coordination of atoms strongly varies in a liquid. Further existing pair signatures are typical for atomic short-range order allowing for a high packing density of atoms, but which cannot be continued to yield regular, periodic structures. Among these are, for example, clusters of 13 atoms, consisting of 12 atoms on the corners of an icosahedron surrounding a central atom, which participates in twelve 555 pairs with its neighboring atoms.

We have carried out the CNA for liquid Al during the cooling process from 1300 K down to 600 K. The resulting different pair signatures are shown in Fig. 5. At 1300 K the part of signatures representing close-packed local structures is smaller than 5%, whereas 50% of all bound atom pairs have less than four common neighbors. This reflects the high percentage of atoms with low coordination numbers compared to the case of close-packed structures.

When cooling below the thermodynamic melting temperature the number of pairs of atoms with a close-packed local environment increases over 25% at 600 K. As a consequence the part of pair signatures of atoms with a non-filled first neighbor shell decreases. But what is remarkable and in agreement with the experimental observation (Schenk *et al.*, 2002) is the fact that in the undercooled liquid 433 and 544 signatures are stronger represented than close-packed local structures. These (433 and 544) signatures appear when several fragments of atoms at tetrahedral corners meet at a tetrahedral edge. The corresponding polytetrahedral structures, which consist of three tetrahedrons, lead to the 433 signatures, whereas 544 signatures describe structures consisting of four such tetrahedrons. By deforming the bonds of the latter polytetrahedral structure a pentagonal bipyramid can be built, which gives rise to a 555 signature of the pair of atoms at the lower and upper corners of this structure. Therefore, all polytetrahedral structures, in particular those with 544 signature, can be regarded as precursors of local icosahedral fragments. As the Fig. 5 shows local structures with 555 signature appear more frequently than close-packed local structures, i.e.,

icosahedrons and fragments of icosahedrons dominate in the undercooled liquid at low temperatures. At 1300 K these 555 signatures appear with an abundance of only 1% which increases to 13% at 600 K in the undercooled liquid melt.

The results confirm earlier observations by Jónsson and Andersen (1988) of the importance of icosahedral local structures in undercooled Lennard-Jones liquids. In contrast to the anti-correlation between the abundance of close-packed and icosahedral local structures in the work of Jónsson and Andersen (1988) our simulations show that in metallic liquid melts the tendency for the nucleation of the crystalline structure is not suppressed by the formation of icosahedral local structures, but is only hindered.

5. CONCLUSIONS

In this work we presented MD simulations of liquid Al with an emphasis on changes of atomic short-range order in the undercooled phase. Such investigation requires knowledge of the thermodynamic melting point of the system which we determined with the help of simulations for the coexisting (solid and liquid) phases (so called two-phase simulations). This is a rapid and very precise method to determine the melting point regardless of the nature of the interacting atomic potential used in the simulations. For pure Al we obtained a melting temperature of 1028 K, which deviates by ca. 100 K from the experimental value of 933 K. This lies within the range of deviations obtained for the melting temperature of Al by other groups (Mei and Davenport, 1992; Morris *et al.*, 1994) and also in the range of deviations obtained in simulations using EAM potentials for other metals (Foiles and Adams, 1989).

The investigations of the local structures in the undercooled Al melt have shown that the local structures with crystal symmetry do not dominate; local structures with fivefold symmetry are as abundant as the other symmetries. The existence of such structures having fivefold symmetry, which cannot be continued to a regular periodic structure, is one of the possibilities to explain the phenomenon of undercooling of liquid melts. The transformation of these icosahedral fragments into crystalline fragments is only possible by overcoming an energy barrier, which considerably slows down the nucleation of the solid phase, and suppresses it in the span of time used in the molecular-dynamics simulations.

References

- Allen, M. P. and D. J. Tildesley (1987). *Computer Simulation of Liquids*. Clarendon Press, Oxford.
- Ben David, T., Y. Lereah, G. Deutscher, R. Kofman *et al.* (1995). Solid-liquid transition in ultra-fine lead particles. *Phil. Mag. A*, **71**, 1135.
- Binder, H. H. (1999). *Lexikon der chemischen Elemente – Das Periodensystem in Fakten, Zahlen und Daten*. S. Hirzel Verlag, Stuttgart.
- Buffat, P. and J.-P. Borel (1976). Size effect on the melting temperature of gold particles. *Phys. Rev. A*, **13**, 2287.
- Coombes, C. J. (1972). The melting of small particles of lead and indium. *J. Phys. F: Metal Phys.*, **2**, 441.
- Daw, M. S. and M. I. Baskes (1984). Embedded-atom method: Derivation and application to impurities, surfaces, and other defects in metals. *Phys. Rev. B*, **29**, 6443.
- DiMasi, E., H. Tostmann, O. G. Shpyrko, M. Deutsch *et al.* (2000). Surface induced order in liquid metals and binary alloys. *J. Phys.: Condens. Matter*, **12**, 209.
- DiMasi, E., H. Tostmann, O. G. Shpyrko, P. Huber *et al.* (2001). Pairing interactions and gibbs adsorption at the liquid Bi-In surface: A resonant X-ray reflectivity study. *Phys. Rev. Lett.*, **86**, 1583.
- Faken, D. and H. Jónsson (1994). Systematic analysis of local atomic structure combined with 3D computer graphics. *Comp. Mat. Sci.*, **2**, 279.
- Faupel, F., W. Frank, M.-P. Macht, H. Mehrer *et al.* (2003). Diffusion in metallic glasses and supercooled melts. *Rev. Mod. Phys.*, **75**, 237.
- Foiles, S. M. and J. B. Adams (1989). Thermodynamic properties of fcc transition metals as calculated with the embedded-atom method. *Phys. Rev. B*, **40**, 5909.
- Frank, F. C. (1952). Supercooling of liquids. *Proc. R. Soc. London A*, **215**, 43.
- Grabowski, S. P., K. Kadau and P. Entel (2002). Atomistic modeling of diffusion in aluminum. *Phase Transitions*, **75**, 265.
- Holland-Moritz, D., T. Schenk, R. Bellissent, V. Simonet *et al.* (2002). Short-range order in undercooled Co melts. *J. Non-Cryst. Solids*, **312–314**, 47.

- Honeycutt, J. D. and H. C. Andersen (1987). Molecular dynamics study of melting and freezing of small Lennard-Jones clusters. *J. Phys. Chem.*, **91**, 4950.
- Jónsson, H. and H. C. Andersen (1988). Icosahedral ordering in the Lennard-Jones liquid and glass. *Phys. Rev. Lett.*, **60**, 2295.
- Kresse, G. and J. Furthmüller (1996). Effective iterative schemes for *ab initio* total-energy calculations using a plane wave basis set. *Phys. Rev. B*, **54**, 11169.
- Lamparter, P. and S. Steeb (1998). Structure of amorphous and molten alloys. In R. W. Cahn, P. Haasen and E. J. Kramer, editors, *Materials Science and Technology*, volume 1, chapter 4, 217. VCH, Weinheim.
- Maret, M., F. Lancçon and L. Billard (1993). Bond-orientational order in liquid aluminum₈₀-transition metal₂₀ alloys. *J. Phys. I (France)*, **3**, 1873.
- Mei, J. and J. W. Davenport (1992). Free-energy calculations and the melting point of Al. *Phys. Rev. B*, **46**, 21.
- Morris, J. R. and X. Song (2002). The melting line of model systems calculated from coexistence simulations. *J. Chem. Phys.*, **116**, 9352.
- Morris, J. R., C. Z. Wang, K. M. Ho and C. T. Chan (1994). Melting line of aluminum from simulations of coexisting phases. *Phys. Rev. B*, **49**, 3109.
- Pawlow, P. (1909a). Über die Abhängigkeit des Schmelzpunktes von der Oberflächenenergie eines festen Körpers. *Z. Phys. Chem.*, **65**, 1.
- Pawlow, P. (1909b). Über die Abhängigkeit des Schmelzpunktes von der Oberflächenenergie eines festen Körpers (Zusatz.). *Z. Phys. Chem.*, **65**, 545.
- Rapaport, D. C. (1995). *The Art of Molecular Dynamics Simulation*. Cambridge University Press, Cambridge.
- Reichert, H., O. Klein, H. Dosch, M. Denk *et al.* (2000). Observation of five-fold local symmetry in liquid lead. *Nature*, **408**, 839.
- Reutzel, S. and D. M. Herlach (2003). Magnetic properties of undercooled Co and Co-Au alloy melts. *Verhandl. DPG*, **38**, 5/278.
- Rieth, M. (2003). *Nano-Engineering in Science and Technology – An Introduction to the World of Nano-Design*. World Scientific, Singapore.

- Rößler, U. K. and H. Teichler (2000). Molecular dynamics simulations of supercooled and amorphous $\text{Co}_{100-x}\text{Zr}_x$: Atomic mobilities and structured properties. *Phys. Rev. E*, **61**, 394.
- Schenk, T., D. Holland-Moritz, V. Simonet, R. Bellissent *et al.* (2002). Icosahedral short-range order in deeply undercooled metallic melts. *Phys. Rev. Lett.*, **89**, 075507.
- Simonet, V., F. Hippert, M. Audier and R. Bellissent (2002). Local order in liquids forming quasicrystals and approximant phases. *Phys. Rev. B*, **65**, 024203.
- Simonet, V., F. Hippert, H. Klein, M. Audier *et al.* (1998). Local order and magnetism in liquid Al-Pd-Mn alloys. *Phys. Rev. B*, **58**, 6273.
- Steinhardt, P. J., D. R. Nelson and M. Ronchetti (1981). Icosahedral bond orientational order in supercooled liquids. *Phys. Rev. Lett.*, **47**, 1297.
- Tostmann, H., E. DiMasi, P. S. Pershan, B. M. Ocko *et al.* (2000). Microscopic structure of the wetting film at the surface of liquid Ga-Bi alloys. *Phys. Rev. Lett.*, **84**, 4385.
- Turnbull, D. (1950). Formation of crystal nuclei in liquid metals. *J. Appl. Phys.*, **21**, 1022.

Figure Captions

Figure 1:

The potential energy $E_{\text{pot}}(V)$ per atom as a function of the volume V per atom. Curves for two different EAM potentials fitted to the experimental data are shown; for details of the EAM potentials see Grabowski *et al.* (2002). The $E_{\text{pot}}(V)$ curve obtained from the EAM potential fitted to experimental data only is represented by a dashed line, whereas the full line represents $E_{\text{pot}}(V)$ obtained from the EAM potential subject to an additional fit to *ab initio* data: The filled circles represent $E_{\text{pot}}(V)$ calculated with VASP (*Vienna Ab Initio Simulation Package*) using ultrasoft Vanderbilt pseudopotentials (Kresse and Furthmüller, 1996).

Figure 2:

Total energy per Al atom E as a function of temperature T . Results have been taken from the final states of the two-phase simulations with a spherical solid particle of diameter 46.6 Å embedded in liquid Al. The sharpness of the solid-liquid transition allows a precise determination of the melting temperature of the particle, which is $T_m = 908.5 \pm 0.5$.

Figure 3:

Melting temperature T_m as a function of the particle diameter d for initially spherical solid Al particles embedded in liquid Al (two-phase MD simulations). If we assume a linear behavior of $T_m(d^{-1})$ we may extrapolate from the data the bulk melting point, which gives $T_B = 1028$ K ($T_B^{\text{exp}} \approx 933$ K).

Figure 4:

Melting temperature of free Al nano-clusters as a function of the diameter d (filled circles) and of $1/d$ (open squares). The extrapolated melting temperature of bulk Al obtained from the linear variation of $T_m(d^{-1})$ amounts to 1030 K and is slightly higher than the corresponding T_B value of 1028 K obtained from the two-phase simulations.

Figure 5:

Variation of the relative numbers of bonded pairs with different CN signatures (see text) on cooling. Curves have been normalized to the total number of bonded pairs at each temperature, the number of which increases by 49% on cooling. The simulations confirm the experimental trend (Schenk *et al.*, 2002) that the icosahedral short-range order strongly increases with the de-

gree of undercooling.

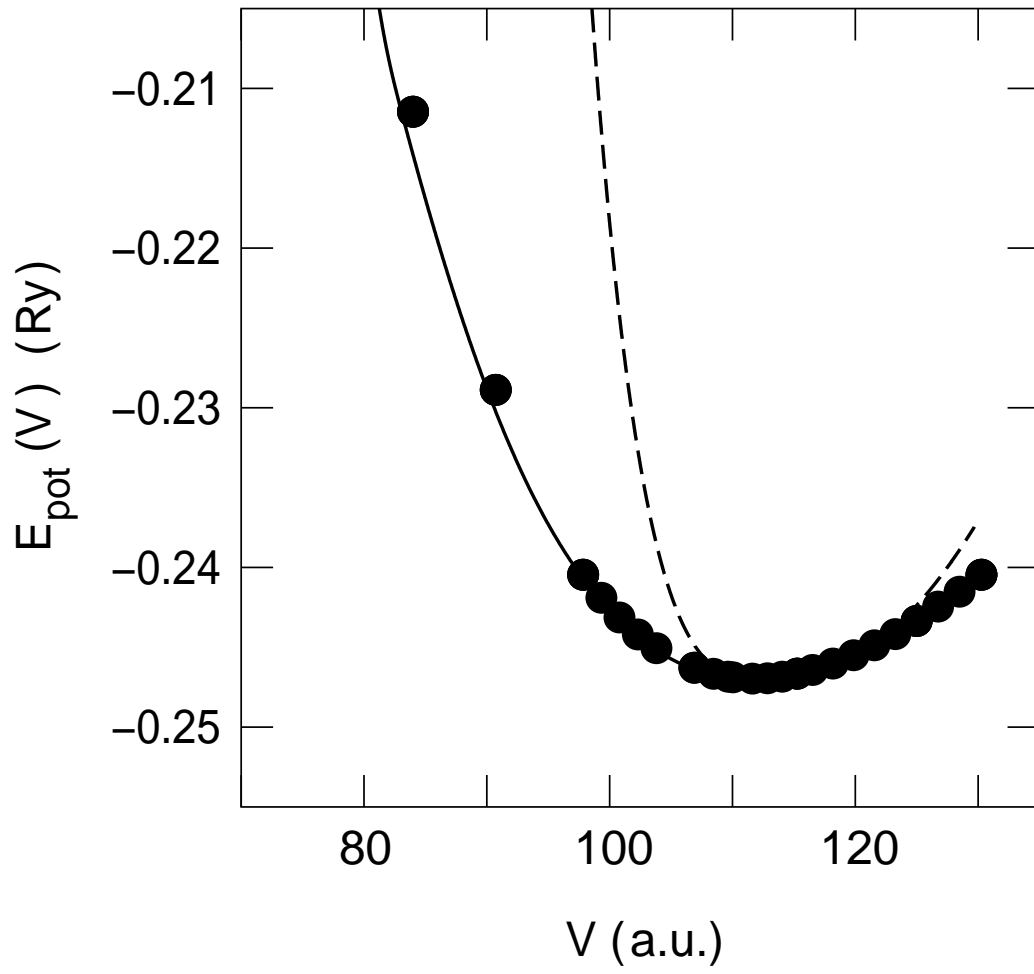


Figure 1: M. Kreth *et al.*

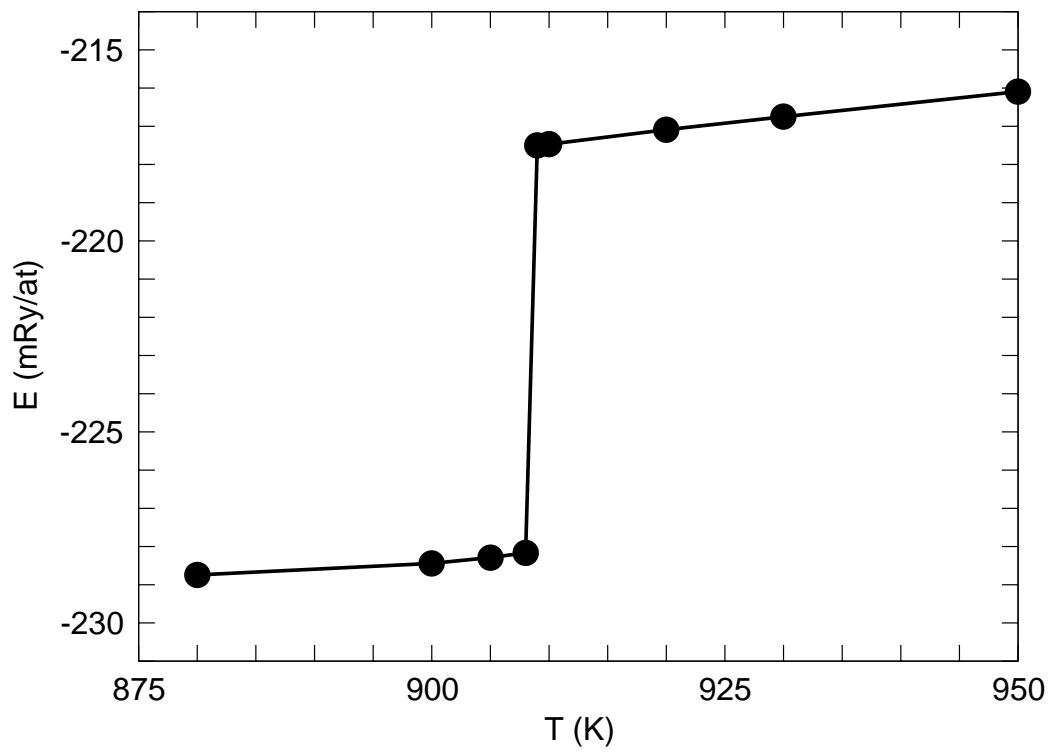


Figure 2: M. Kreth *et al.*

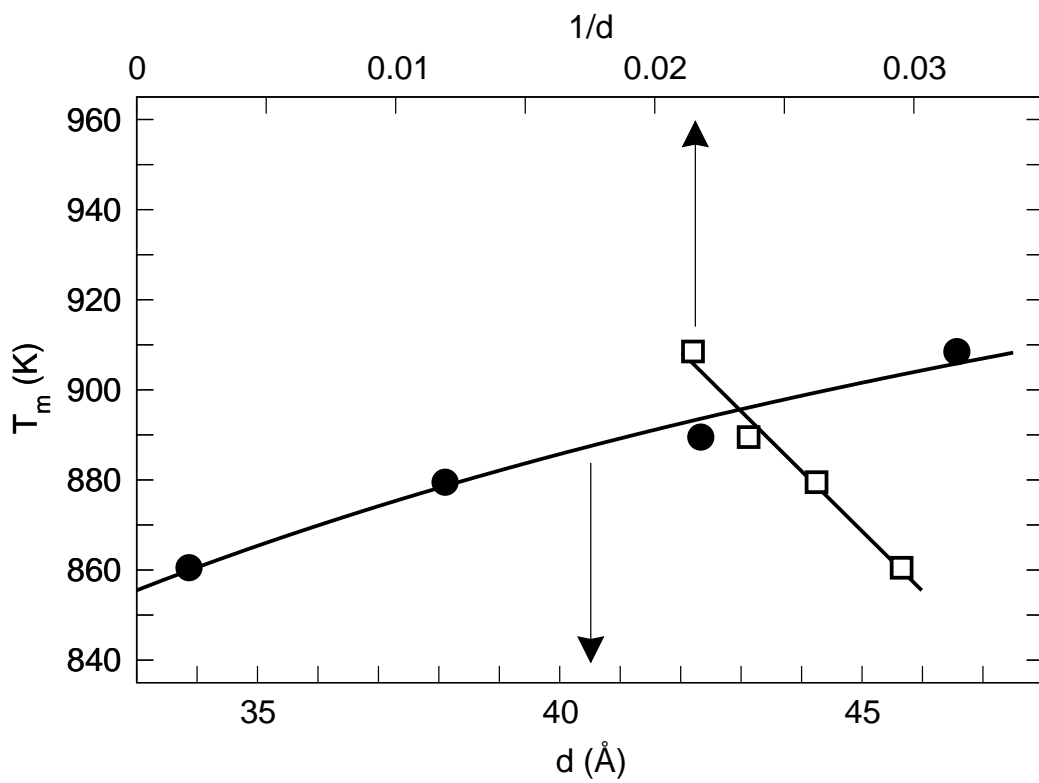


Figure 3: M. Kreth *et al.*

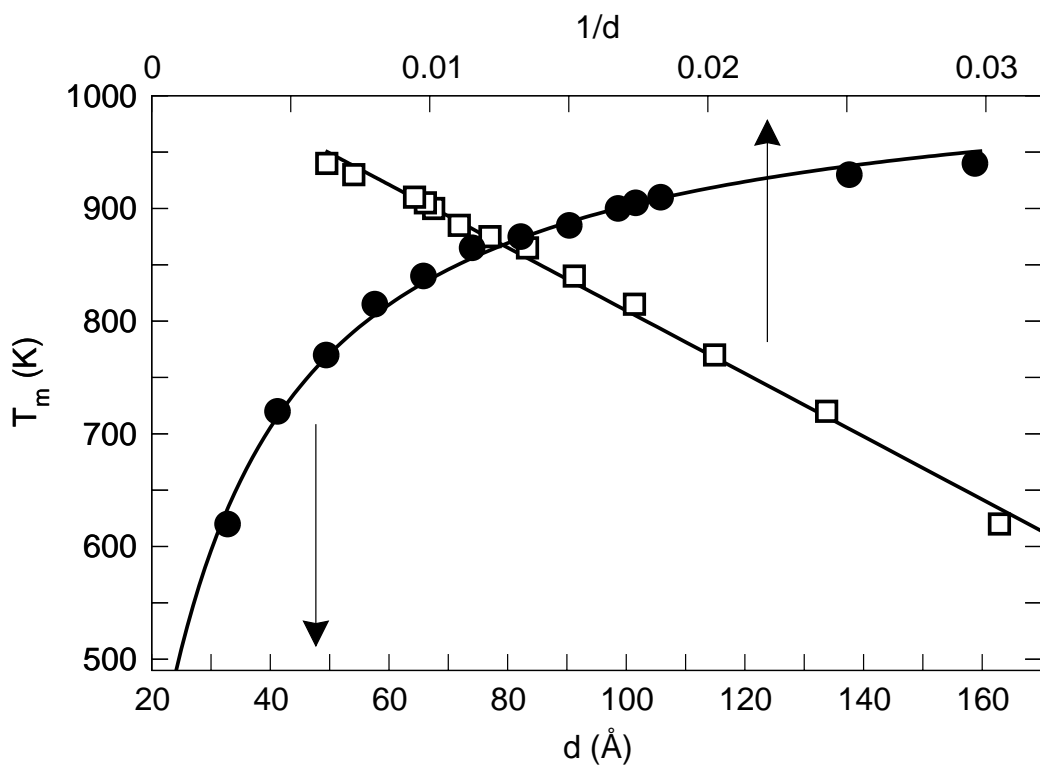


Figure 4: M. Kreth *et al.*

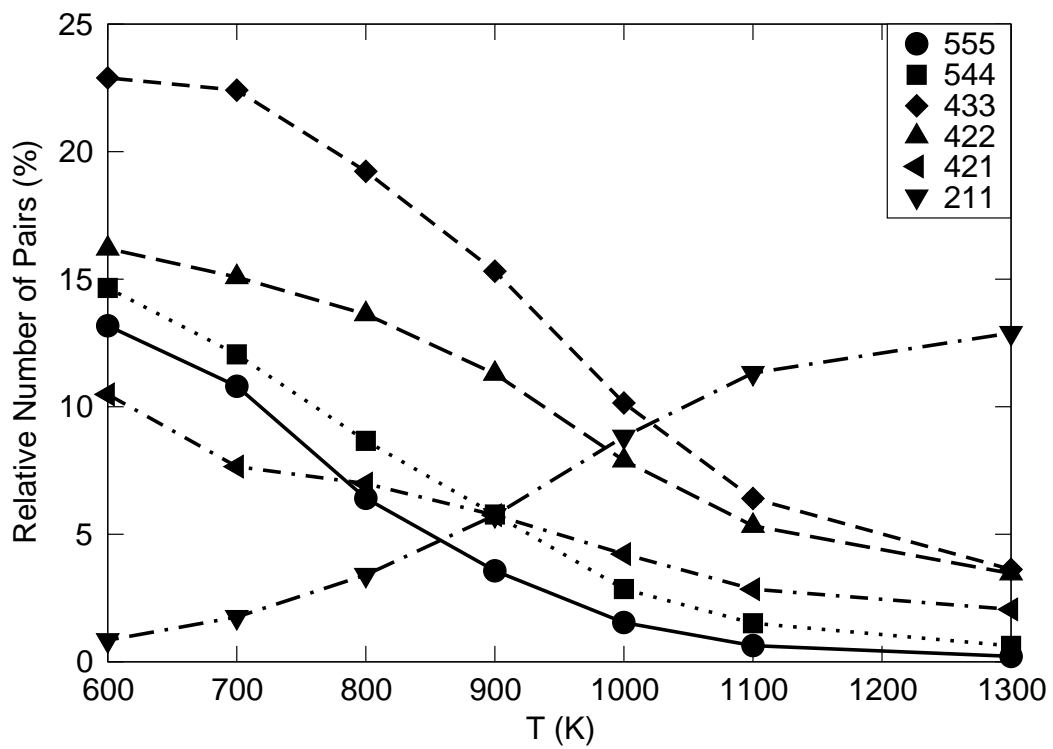


Figure 5: M. Kreth *et al.*